



Open Archive Toulouse Archive Ouverte





OATAO is an open access repository that collects the work of Toulouse researchers and makes it freely available over the web where possible

This is an author's version published in: <https://oatao.univ-toulouse.fr/27454>

Official URL:

<https://doi.org/10.1016/j.proci.2020.06.378>

To cite this version:

Laera, Davide and Agostinelli, Pasquale Walter and Selle, Laurent  and Cazères, Quentin and Oztarlik, Gorkem  and Schuller, Thierry  and Gicquel, Laurent Y.M. and Poinso, Thierry  *Stabilization mechanisms of CH₄ premixed swirled flame enriched with a non-premixed hydrogen injection.* (2021) Proceedings of the Combustion Institute, 38 (4). 6355-6363. ISSN 1540-7489 .

Any correspondence concerning this service should be sent to the repository administrator: tech-oatao@listes-diff.inp-toulouse.fr

Stabilization mechanisms of CH₄ premixed swirled flame enriched with a non-premixed hydrogen injection

D. Laera^{a,b,*}, P. W. Agostinelli^{a,c}, L. Selle^b, Q. Cazères^a, G. Oztarlik^b, T. Schuller^b, L. Gicquel^a, T. Poinsot^b

^aCERFACS, 42 avenue Gaspard Coriolis, 31057 Toulouse, France

^bInstitut de Mécanique des Fluides de Toulouse, IMFT, Université de Toulouse, CNRS, 31400 Toulouse, France

^cSafran Helicopter Engines, Bordes, France

Abstract

High-fidelity Large Eddy Simulations (LES) are performed to study the effect of hydrogen injection on a lean turbulent CH₄/Air premixed flame. An Analytically Reduced Chemistry (ARC) mechanism is used to achieve a detailed description of CH₄/Air-H₂ chemistry. First, a validation of this kinetic scheme against the detailed GRI-Mech 3.0 mechanism is presented considering both simplified and complex transport properties. When hydrogen is added to the mixture, large variations of the mixture Prandtl and of the N₂ Schmidt numbers are observed depending on the local species concentration, features that are missed by simplified models. LES is then applied to study the structure and stabilization mechanisms of a lean ($\phi = 0.8$) premixed CH₄/Air swirled flame enriched with hydrogen by using different transport modeling strategies. First, the fully premixed CH₄/Air case is considered and results are found to validate the LES approach. In agreement with experiments, a classical V-shape flame is stabilized in the low-velocity region near the flame holder created by a central recirculation zone (CRZ). Then, hydrogen enrichment is achieved injecting 2% of the CH₄ thermal power with a central fuel injection lance. Both premixed and diffusion flame branches are present in this case, impacting flame stabilization and angle. The flame root the main premixed flame stabilized by a diffusion flame kernel created by the injected hydrogen reacting with the oxygen in excess of the premixed stream. Moreover, the H₂ consumed with the remaining oxygen in burnt gases leads to the formation of a second flame branch inside the CRZ which is responsible of an increase of the flame angle. Given the high concentration of hydrogen, an impact of the molecular transport models is observed on the flame lift-off height highlighting the importance of using complex transport properties in any LES involving hydrogen combustion.

Keywords:

H₂ enriched flame, Flame stabilization mechanism, Large Eddy Simulations, Transport properties

*Corresponding author:

Email address: laera@cerfacs.fr (D. Laera)

1. Introduction

Stringent regulations on pollutants emissions from combustion devices to comply with EU objectives make the development of low-emission combustors a major design challenge for aero and land-based gas turbines. In this scenario, the combination of hydrogen with standard carbon-based fuels is actually considered as one of the most promising technical solution for clean combustion [1]. Indeed, lean flame stabilization is enhanced by the hydrogen high flame speed and its wide flammability range [2, 3]. Furthermore, hydrogen offers no emissions of HC or CO₂ [3].

For these reasons, multiple numerical and experimental studies have been carried out to study the impact of hydrogen addition on methane/air flames. Experiments and Direct Numerical Simulations (DNS) on laminar flame speeds [2, 4–6], lean and anomalous blow-off [7, 8], stabilization mechanisms and instabilities [9] have been performed for canonical flames. More realistic swirled configurations have been also investigated. Schefer *et al.* [10] studied the impact of hydrogen on flame stability and blowout for a lean premixed swirl-stabilized flame showing that the addition of a moderate amount of hydrogen to the methane/air mixture increases the peak OH concentration with a significant change in the flame structure which is shorter and more robust. A non-premixed unconfined configuration was investigated by Cozzi and Coghe [11]. Fuel mixtures containing a variable volumetric fraction of CH₄ and H₂ are injected in a swirling air flow. Again with hydrogen addition a shorter and narrowed blue flame located closer to the burner head was observed. The impact of H₂ on emissions was also extensively studied. As an example, a decrease of NO_x level, if compared with a corresponding diffusion flame under same operating conditions, was observed for a fuel-lean confined swirl-stabilized methane-air flame by Kim *et al.* [12]. Recently, the impact of hydrogen enrichment on the shape of confined swirled flames was investigated by Guiberti *et al.* [13] and Shanbhogue *et al.* [14]. In this study, the probability of stabilizing a M-flame increases with the H₂ concentration in the combustible mixture. From a numerical point of view, the appeal of high-fidelity LES (e.g., see Ref. [15]) is increasing for these studies given their higher accurate prediction capabilities at a reasonable cost if compared to cheaper Unsteady Reynolds Averaged Simulations (URANS) and unaffordable DNS. Refs. [16, 17] report some examples of studies on academic configurations and, very recently, the methodology was also extended to a full-scale gas turbine combustor [18]. In all these previous

studies hydrogen is always considered fully premixed with the fuel mixture. Fewer are the investigations of direct H₂ injection in the combustion chamber. Indeed, in this case the pure H₂ flame will behave as a classical pilot flame typical of land-based gas turbines or aero-engines [1] opening new questions on the resulted flame structure and stabilization mechanisms.

The present work aims at filling the observed gap of knowledge by performing experiments and high-fidelity LES of the impact of H₂ injection on flame structure and stabilization of a confined lean swirling flame. For this specific objective, simulations are performed coupling the LES solver AVBP with an Analytically Reduced Chemistry (ARC) scheme for CH₄/Air-H₂ chemistry. The impact of considering simplified or complex transport properties is also discussed. This is a topic well developed for classical single-fuel systems, but less investigated in case of bi-fuel configurations [19]. With respect to a classical lean CH₄/Air premixed swirled flame, simulations reveal that both premixed and diffusion flames are present when hydrogen is injected, impacting flame stabilization mechanisms and angle.

2. Experimental setup and Numerical model

The numerical simulations carried out in this work refer to the experiments performed in the MIRADAS combustor developed at IMFT laboratory, CNRS (Toulouse, France) [20]. Figure 1(a) reports a schematic of the combustor. A methane/air mixture is well premixed before entering the upstream longitudinal plenum. After being pushed through a radial swirler consisting of eight channels of $r = 2.25$ mm radius oriented at 15° with respect to the burner axis, the mixture enters a 100 mm long quartz flame tube through an annular gap of inner and outer diameters equal to 6 and 12 mm, respectively. Hydrogen is conveyed directly in the chamber through a 4 mm pilot lance passing along the entire axis of the plenum. At the inlet of the combustion chamber, the two streams are separated by a thin annular lip of 1 mm (Fig. 1(a)). Two operating points are studied in this work. First, a perfectly premixed methane/air mixture with an equivalence ratio of $\phi = 0.8$ and thermal power of $P_{th} = 3.96$ kW is considered (case **REF**). Then, the flame is enriched through the pilot lance injecting a mass flow of hydrogen corresponding to the 2% of the CH₄ thermal power of case **REF** (case **PH2**). More details on the two operating conditions are summarized in Tab. 1. For **PH2**, the methane mass flow rate is slightly changed in order to keep the total thermal power constant. Note that this specific variation is so small that no significant change in the

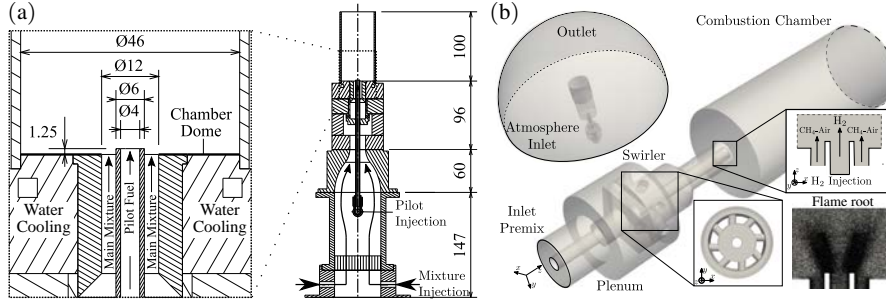


Figure 1: (a) Schematic of the MIRADAS experimental rig. (b) Numerical setup with details of the computational grid at the flame root.

global equivalence ratio is achieved. For both cases, in the annular premix passage a well established turbulent flow reaches a Reynolds number of $Re_{pre,D_h} \approx 7000$ using the equivalent hydraulic diameter $D_h = 6$ mm of the annular channel. The hydrogen flow is always laminar and $Re_{H_2} \approx 25$.

Case	Main		Pilot	Global
	\dot{m}_{Air} (g/s)	\dot{m}_{CH_4} (g/s)	\dot{m}_{H_2} (g/s)	ϕ
REF	1.693	$7.912 \cdot 10^{-2}$	-	0.8
PH2	1.693	$7.754 \cdot 10^{-2}$	$6.597 \cdot 10^{-4}$	≈ 0.8

Table 1: Mass flow rates of air, methane and hydrogen and respective global equivalence ratios for the two operating conditions.

The domain used for the LES (Fig. 1(b)) has been discretized using an unstructured mesh which has been refined until a grid-independent solution is obtained. The final computational grid consists of approx. 23M tetrahedral elements. Note that to correctly capture the flame stabilization mechanisms, the grid is designed with a refinement of $\Delta x \approx 80 \mu m$ assuring approximately twelve points in the separation zone between the two fuel lines and in the finest region positioned at the flame root (zoom box in Fig. 1(b)). Another refinement region with $\Delta x \approx 300 - 350 \mu m$ is located further downstream. Turbulent combustion is modeled using the dynamic TFLES model, which imposes a flame thickening everywhere a reactive zone is detected by a flame sensor [21]. Note that, once a target flame resolution is prescribed (i.e. 5 points in the flame front are specified for the present LES), the dynamic formulation of TFLES does not impose a constant level of thickening everywhere. Indeed, the model thickens the flame at the level that is required to reach the target resolution considering the local mesh size and laminar flame thickness (i.e. $\Delta_l \approx 550 \mu m$ in the present case). As a consequence, a thickening factor equals to unity is applied in the zones where the flame is already sufficiently resolved. This is typically what is happening close to the burner lips. Simulations are performed using AVBP (www.cerfacs.fr/avbp7x/), an explicit

cell-vertex parallel code solving compressible reacting flows with the use of the SIGMA turbulent closure for the subgrid Reynolds stresses [22]. A third order accurate Taylor-Galerkin scheme [23] is adopted for discretisation of the convective terms. Inlets and outlets are treated with the Navier-Stokes Characteristic Boundary Conditions [24] imposing the mass flow rates (Tab. 1), and ambient pressure, respectively. For both operating conditions, a measured temperature of $T_{bkpl} = 450$ K and $T_{lip} = 720$ K is fixed, respectively, at the chamber backplane and separator lip. Combustion chamber wall heat losses are taken into account imposing a temperature profile measured with a movable thermocouple from the external side of the flame tube and a thermal resistance of $R_{w,cc} = 9 \cdot 10^{-4} m^2 K/W$ computed assuming a thermal conductivity $\lambda = 2.17$ W/mK for the 2 mm thick quartz wall.

3. Chemistry and Transport properties

The $CH_4/Air-H_2$ chemistry is described by an ARC mechanism comprising 20 species, 166 reactions, and 9 quasi-steady state species derived from GRI-Mech 3.0 using ARCANE (www.chemistry.cerfacs.fr/en/arcane). A complete description of the ARC mechanisms is reported in section A of the supplementary materials. To validate the kinetic schemes, Cantera (www.cantera.org) calculations of a 1D-counterflow H_2 diffusion flame against equilibrium products from a lean CH_4/Air flame is presented in Fig. 2. The detailed GRI-Mech 3.0 scheme with multicomponent transport and Soret effect [25] is then compared to the reduced ARC mechanism using both simplified and mixture average transport properties models. The latter model is the standard approach for complex transport. An alternative often present in LES codes is the simplified approach which consists in determining the viscosity from the Sutherland's law and deducing the mixture heat conductivity using a constant Prandtl number while each

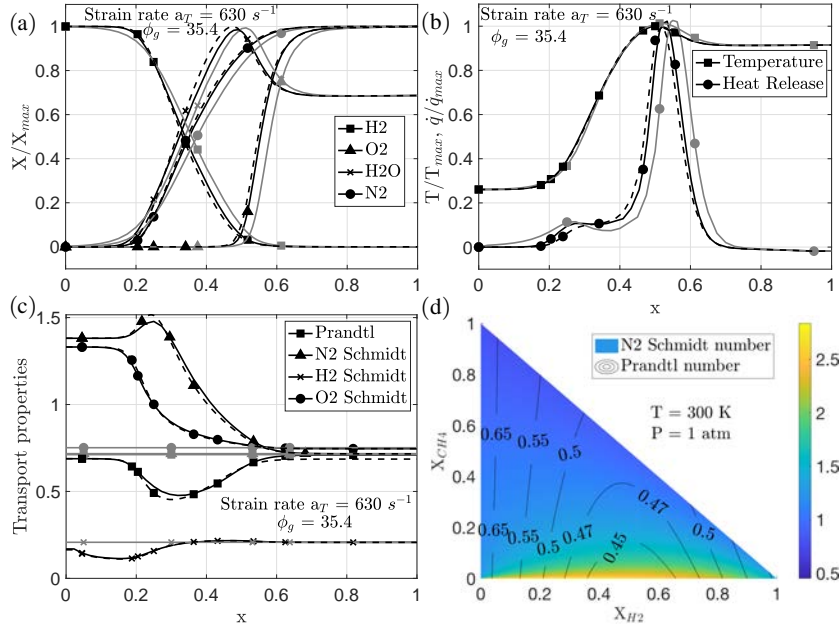


Figure 2: (a-c) Comparison between flame structures computed with Cantera using GRI-Mech 3.0 mechanism including multicomponent transport and Soret effect (dashed lines), the ARC scheme with a mixture transport model (dark line) and simplified transport model (light line), for a counterflow diffusion flame of H₂ against the equilibrium burnt gases from lean ($\phi = 0.8$) CH₄/Air premixed flame. Normalized profiles of (a) mass fraction of selected species, (b) temperature and heat release rate; (c) profiles of the transport properties. Computation inputs are: $p = 1$ bar, injection temperature of $T_{H_2}^i = 570$ K and exhaust gas temperature $T_g^i = 2000$ K. (d) Isolines of the Prandtl number and contour map of N₂ Schmidt number in ternary mixture of H₂, CH₄ and N₂ as a function of composition.

species diffusivity relies on a constant Schmidt number. The calculation is performed with hydrogen injected at 2.8 m/s and burned gases injected at 3.5 m/s separated by a reference distance of $\delta = 10$ mm leading to a strain rate $a_T = 630$ s⁻¹ [26]. This diffusion flame mimics the H₂ combustion process of the final target configuration close to the burner outlet. The heat release profiles obtained with the three mechanisms present two reaction peaks, a primary peak in the rich side of the flame, very close to H₂ injection point and a second one, much larger, in the stoichiometric region of the flame. Normalized species, temperature and heat release rate profiles comparisons show perfect agreement between GRI-Mech 3.0 scheme and the ARC scheme with complex transport while showing only satisfactory agreement with a simplified transport model (Fig. 2(a-b)). Figure 2(c) shows the Prandtl (Pr) and Schmidt (Sc) numbers of selected species present in the 1D-counterflow diffusion flame confirming the variability present in this problem. It is noted that the GRI-Mech 3.0 scheme and the ARC scheme with complex transport predict a Pr number dropping from 0.7 to 0.43 in the region just before the heat release rate peak, i.e., a region where H₂ and N₂ form a binary mixture of almost equal molar fraction. This leads to higher thermal con-

ductivity and hence to a lower temperature peak in the flame if compared to constant transport property case. Finally, the N₂ Schmidt and the mixture Prandtl number in a ternary mixture of N₂, H₂ and CH₄ are reported in Fig. 2(d). By looking at the isolines of the Prandtl number it can be noticed that Pr is a strong function of the H₂ molar fraction and takes its minimum values when H₂ is present in a binary mixture with N₂¹ with almost equal molar fractions. Focusing on the Schmidt number, both the 1D-counterflow diffusion flame of Fig. 2(c) and the ternary mixture of Fig. 2(d) show a variation of the N₂ Schmidt number from 2 when it diffuses in H₂ to only, 0.7 when it diffuses in other gases. Variations of the Schmidt numbers of other species, even if present, do not influence combustion since they are rapidly consumed (e.g. O₂, CH₄). Reduced diffusion of N₂ in H₂ due to the increase of Sc, decreases the local H₂ molar fraction and the resulted flame will be shifted toward the H₂ side. Vice-versa, when simplified transport is used, N₂ diffuses more in the H₂ side leading to a flame

¹It should be also noticed that similar results would have been achieved with a mixture of H₂ with other heavy components such as O₂. However, in the present configuration, oxygen is immediately burned so its concentration is extremely low in the zones where hydrogen is present. For this reason, N₂ is considered in Fig. 2(d).

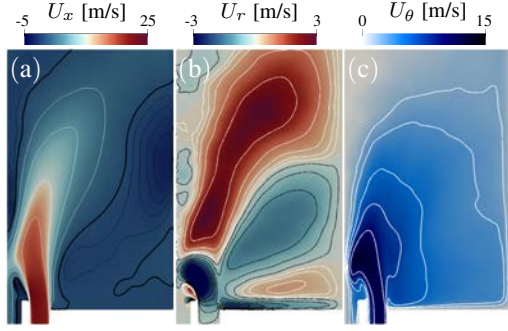


Figure 3: Time and angle average contours of axial U_x (a), radial U_r (b) and tangential U_θ (c) velocity components. Black isolines indicate negative values, while positive velocities are in white. The thick black isoline in the axial velocity map corresponds to $U_x = 0$.

shifted towards the oxidant side as shown in Fig. 2(b). Variable Pr and N_2 Sc number polynomial functions of the molar fractions X_{CH_4} , X_{N_2} and X_{H_2} are implemented in AVBP and used for the following simulations. These corrections allow to match the complex transport model perfectly for such flames. Expressions of these functions are reported in section B of the supplementary materials.

4. Results and discussion

Before discussing the reactive simulations, LES time averaged contours of axial U_x , radial U_r and tangential U_θ velocities of the non-reacting flow are shown in Fig. 3(a-c). The imposed swirl motion is not sufficient to achieve a complete vortex-breakdown. At the exit of the annular channel, a large radial component pushes the jet towards the chamber axis (Fig. 3(b)). As a consequence, the system features a central recirculation zone (CRZ) that is not completely developed as highlighted by the black thick isoline $U_x = 0$ in Fig. 3 (a). A good match with experimental results is obtained for global quantities such as the swirl number computed at the entrance of the combustion chamber ($S_{LES} = 0.35$ against a geometrical value of $S_{th} = 0.3$) and injector head loss ($\Delta_{p,LES} = 480$ Pa against measured $\Delta_{p,exp} = 550$ Pa) confirming the accuracy of the proposed simulations.

4.1. REF case

First, the reactive case **REF** without hydrogen injection (Tab. 1) is discussed. The flame shape obtained taking the line-of-sight (LOS) integration of the CH^* chemiluminescence intensity signal (Fig. 4(a)) is compared with the LOS of the predicted heat release rate (Fig. 4(b)). Both maps are reported normalized with respect to their maximum value. The predicted

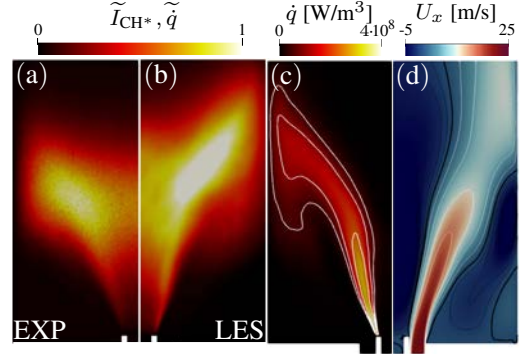


Figure 4: Comparison between the normalized line-of-sight (LOS) integration of measured CH^* chemiluminescence intensity \tilde{I}_{CH^*} (a) and the normalized LOS integration of the heat release rate \tilde{q} from LES (b). Time and angle average contours of heat release rate with $\dot{q} = 40, 100, 200$ MW/m³ isolines (c). Time and angle average contours of axial velocity U_x (d). Black isolines indicate negative values, positive velocities are in white, the thick black line refers to $U_x = 0$.

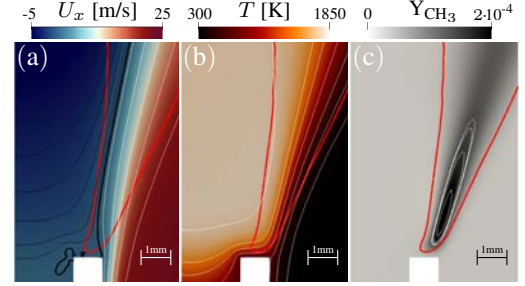


Figure 5: Zoom on the flame root. Isoline of heat release rate (red line) at $\dot{q} = 40$ MW/m³ (10% of the maximum value) plotted over the contours of axial velocity U_x (a), temperature (b), mass fraction of CH_3 (c). In the velocity map, black isolines indicate negative values, positive velocities are in white. The thick black line refers to $U_x = 0$.

global flame shape is in agreement with experiment. No flame is predicted in the corner recirculation zones (CRZ) proving the appropriateness of the assumed thermal boundary conditions. A good match is also found in terms of lift-off distance and flame angle, whereas LES slightly overestimates the flame total extension. The well-established V-shape of the flame is also clearly visible in Fig. 4(c) reporting time and angle average contours of heat release rate. Axial velocity contours are shown in Fig. 4(d). Comparing with the corresponding map for the cold flow (Fig. 3(a)), a proper vortex-breakdown with the formation of a complete and extended CRZ is achieved with combustion.

Zooming now at the flame root allows to discuss the flame stabilization mechanisms. An isoline at 10% of the maximum of the mean heat release rate (red line) is plotted in Fig. 5(a) over the axial velocity map. The swirled flame is stabilized inside the low velocity zone filled with hot gases created by the CRZ on top of the

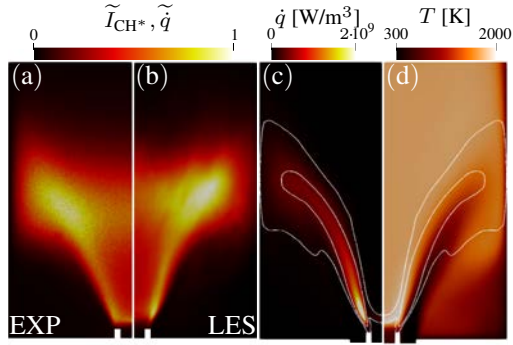


Figure 6: Comparison between the normalized LOS integration of measured CH^* chemiluminescence intensity \tilde{I}_{CH^*} (a) and the normalized LOS integration of the heat release rate \tilde{q} from LES (b). Time and angle average contours of heat release rate (c) and temperature T (d) with isolines (white lines) of $\dot{q} = 200 \text{ MW/m}^3$ (10% of the maximum value) and $\dot{q} = 40 \text{ MW/m}^3$.

separation lip. Plotting the same heat release rate level over the iso-contours of temperature in Fig. 5(b) underlines the fact that flame stabilization happens along a temperature value of $T \simeq 1300 \text{ K}$, which is close to the activation temperature of the reaction leading to the production of CH_3 from methane. Indeed, this species is found to concentrate within the heat release rate isoline (Fig. 5(c)) proving that it is a good indicator of the position of the flame root.

Since no hydrogen is injected, very low X_{H_2} is obtained for this case (not shown), therefore the impact of the transport model is accordingly negligible.

4.2. PH2 case

As soon as H_2 is injected from the pilot channel, the flame structure changes. Focusing on the measurements Fig. 6(a), comparing with the **REF** case (Fig. 4(a)), a more intense zone is observed at the flame root and all along the outer side of the flame facing the CRZ. In agreement with the experiments, LES show high heat release rate in similar areas (Fig. 6(b)). Nevertheless, some differences are observable. A mismatch of approx. 1 mm is indeed noted in the flame lift-off height. This may be due to the lip temperature which was measured in the experiments and imposed in the LES. Time and angle average contours of heat release rate reported in Fig. 6(c) give more insight on the flame structure. Again, if compared to case **REF**, higher mean values of heat release rate are obtained. The isoline of the heat release rate at $\dot{q} = 200 \text{ MW/m}^3$, i.e. at 10% of its maximum value, shows a flame shape similar to the **REF** case (Fig. 4(c)). On the contrary, a flame branch in the CRZ is well detectable by the isoline at $\dot{q} = 40 \text{ MW/m}^3$, i.e. the same level used to indicate the flame

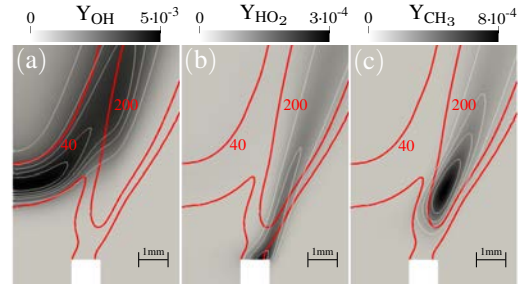


Figure 7: Time average mass fractions of OH , HO_2 and CH_3 at the flame root with isolines of heat release rate (red lines) at $\dot{q} = 40$ and 200 MW/m^3 .

in case **REF**. The central region is therefore hotter, with temperatures that reach 2000 K . A wider flame angle is then achieved, in line with experimental observations.

Looking at mass fractions of OH , HO_2 and CH_3 in the flame root region, high concentrations of OH (Fig. 7(a)) are found within the isolines at $\dot{q} = 40 \text{ MW/m}^3$ suggesting that the injected H_2 is responsible for the heat release in this zone. Similarly, the presence of high concentrations of HO_2 just above the splitter indicates that part of hydrogen is also immediately consumed in that region when a sufficient concentration of H_2 and O_2 is reached (Fig. 7(b)). The high concentration of CH_3 (Fig. 7(c)), instead, indicates that the anchoring point of the CH_4 premixed flame is lifted off with respect to case **REF**. This species is completely enclosed by the higher $\dot{q} = 200 \text{ MW/m}^3$ isoline confirming that, also for this case, CH_4 oxidation drives the mean heat release.

To better understand the interaction between hydrogen and the premix mixture, two Takeno flame indices (FI) [27] are computed. To do so, variables are conditioned by the consumption rates of H_2 and CH_4 , respectively, and then weighted by the magnitude of these variables to underline the regions in which heat release is more relevant:

$$FI_{\text{Fuel}} = |\dot{\omega}_{\text{Fuel}}| \frac{|\nabla_{\text{O}_2} \cdot \nabla_{\text{Fuel}}|}{\|\nabla_{\text{O}_2} \cdot \nabla_{\text{Fuel}}\|} \Big|_{\dot{\omega}_{\text{Fuel}} < 0} \quad (1)$$

Results in the flame root region are reported in Fig. 8. While the Takeno index of CH_4 is always positive, confirming that it burns in premixed mode (Fig. 8(a)), the FI of H_2 detects that hydrogen is consumed in both premixed and diffusion regimes (Fig. 8(b)). A large diffusion reacting layer generated by the reaction of H_2 with residual O_2 in the burned gases is found in the CRZ, confirming the hydrogen nature of this second branch of the flame. At the flame root, a premixed region is predicted detached from the splitter and is believed to be generated by H_2 diffusion from the high concentration

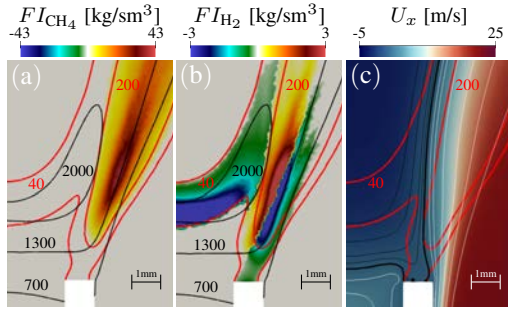


Figure 8: Zoom on the flame root. Computed dimensional Takeno index of CH_4 (a), dimensional Takeno index of H_2 (b) with isolines of temperature (black lines) at $T = 700, 1300$ and 2000 K and heat release rate (red lines) at $\dot{q} = 40$ and 200 MW/m^3 . (c) Contours of axial velocity U_x with isolines of heat release rate (red). Isolines of negative velocity values are in black, positive velocities are in white. The thick black line refers to $U_x = 0$.

zone to the CH_4/Air stream. More interestingly, a second diffusion reacting layer is predicted starting from the splitter wall until the premixed zone. This flame is obviously responsible of the HO_2 concentration previously discussed (Fig. 7(b)) and has a direct role in the stabilization mechanisms of the flame. Indeed, plotting the two heat release rate isolines over the axial velocity field Fig. 8(c), it is possible to notice that differently from case **REF**, the hydrogen diffusion flame stabilizes in the low velocity region. This diffusion kernel appears to support the premixed CH_4 flame that is anchored more downstream in a higher positive velocity region. Observing now the temperature profile (black lines in Fig. 8(a-b)), it is noted that hydrogen oxidation happens in a low temperature zone. The extension of the lower flammability limit temperature is a well-known property of H_2 that is characterized by reactions with low activation energy (such as the one correlated to the HO_2 production) [28]. On the contrary, stabilization of the CH_4/Air flames happens at the same temperature $T \approx 1300$ K value as the **REF** case. This shows that the spatial position of the high heat release zone depends on the axial location of these isolines which is highly impacted by the Prandtl number of the mixture and the N_2 Schmidt number as discussed in section 3.

Indeed, focusing then on the transport properties, Fig. 9(a-b) shows, respectively, the Pr and the N_2 Sc contours in the region in which the H_2 (white lines) molar fraction is relevant. To highlight this result, an instantaneous snapshot of H_2 mass concentration of the current simulation (right) is compared in Fig. 9(c) to an equivalent instant with simplified transport properties (left). Pr and Sc numbers for each transported species of the ARC scheme used for the simplified transport case are listed in section B of the supplementary materials.

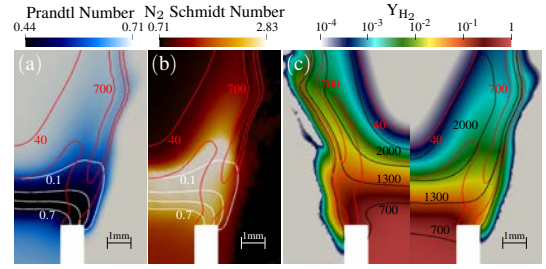


Figure 9: Zoom on the flame root. Instantaneous snapshot of Prandtl number (a) and N_2 Schmidt number (b) with isolines of heat release rate (red lines) at $\dot{q} = 40$ and 700 W/m^3 and H_2 molar fraction (white lines) at $X_{\text{H}_2} = 0.1, 0.3, 0.5$ and 0.7 . (c) Comparison between simplified (left) and complex (right) transport properties computations on an instantaneous snapshot. Mass fraction of H_2 (log scale) is shown together with isolines of heat release rate (red lines) at $\dot{q} = 40$ and 700 MW/m^3 and temperature (black lines) at $T = 700, 1300$ and 2000 K.

In both images, isolines of the temperature field are also reported (black lines). With complex transport properties (Fig. 9(c-right)) the region with high concentration of H_2 moves upstream since N_2 diffuses less from the upper region (i.e. higher Schmidt number). A different diffusion of H_2 , together with a higher thermal conductivity, i.e., lower Prandtl number, have a strong impact on the temperature field, making the hotter region following the movement of H_2 concentration downward. Simplified transport properties (Fig. 9(c-left)) fail to correctly reproduce this mechanism, resulting in a less diffuse temperature field. As a consequence, the low-intense hydrogen reaction zone is more stretched and the CH_4 oxidation is pushed downstream resulting in a lifted flame.

5. Conclusions

In this paper, the impact of non-premixed hydrogen addition on the flame shape and stabilization mechanisms of a swirled methane/air flame has been considered by a numerical analysis. At first, a novel ARC chemical scheme was derived from the detailed GRI-Mech 3.0 to describe the $\text{CH}_4/\text{Air}-\text{H}_2$ combustion reactions. To validate the reduced chemistry model, calculations of a 1D-counterflow H_2 diffusion flame against equilibrium products from a lean CH_4/Air flame were presented for a condition representative of the combustion regime with H_2 injection in the system (**PH2**). At the same time, large changes of the Prandtl and Schmidt numbers altering the transport properties were highlighted when hydrogen is present. In agreement with experiments, H_2 injection is found to have a marginal impact on the general structure of the swirled V-shaped flame, leading only to a more intense reaction at the

flame root and along the outer side of the flame facing the CRZ. New features were also highlighted with LES. Close to the pilot hydrogen injector outlet, a premixed and a diffusion flame branch were identified when hydrogen is injected impacting the flame stabilization and its angle. These two branches could not be observed when pure CH₄ is injected instead of hydrogen [20]. Indeed, at the flame root the main premixed flame is found to be stabilized on a diffusion flame kernel created by the injected hydrogen reacting with the oxygen of the lean premixed stream. Given the high concentration of H₂ in these regions, flame stabilization is found to be strongly influenced by the adopted transport models highlighting the importance of using complex transport properties in any LES involving hydrogen combustion.

Acknowledgements

This project has received funding from the European Research Council Grant Agreement 832248 (SCIROCCO), the MSCA-IF Grant Agreement 843958 (CLEANERFLAMES) and the H2020-MSC-ITN Grant Agreement 766264 (MAGISTER). HPC resources from CALMIP (Grant P19070) are also acknowledged.

References

- [1] S. Taamallah, K. Vogiatzaki, F. Alzahrani, E. Mokheimer, M. Habib, A. Ghoniem, Fuel flexibility, stability and emissions in premixed hydrogen-rich gas turbine combustion: Technology, fundamentals, and numerical simulations, *Appl. Energy* 154 (2015) 1020–1047.
- [2] T. Boushaki, Y. Dhué, L. Selle, B. Ferret, T. Poinso, Effects of hydrogen and steam addition on laminar burning velocity of methane-air premixed flame: Experimental and numerical analysis, *Int. J. Hydrogen Energy* 37 (2012) 9412–9422.
- [3] H. Guo, G. J. Smallwood, F. Liu, Y. Ju, Ö. L. Gülder, The effect of hydrogen addition on flammability limit and NO_x emission in ultra-lean counterflow CH₄/air premixed flames, *Proc. Combust. Inst.* 30 (2005) 303–311.
- [4] V. Di Sarli, A. D. Benedetto, Laminar burning velocity of hydrogen–methane/air premixed flames, *Int. J. Hydrogen Energy* 32 (2007) 637–646.
- [5] Z. Chen, Effects of hydrogen addition on the propagation of spherical methane/air flames: A computational study, *Int. J. Hydrogen Energy* 34 (2009) 6558–6567.
- [6] S. Bougrine, S. Richard, A. Nicolle, D. Veynante, Numerical study of laminar flame properties of diluted methane-hydrogen-air flames at high pressure and temperature using detailed chemistry, *Int. J. Hydrogen Energy* 36 (2011) 12035–12047.
- [7] C. Jiménez, D. Michaels, A. F. Ghoniem, Stabilization of ultra-lean hydrogen enriched inverted flames behind a bluff-body and the phenomenon of anomalous blow-off, *Combust. Flame* 191 (2018) 86–98.
- [8] Y. J. Kim, B. J. Lee, H. G. Im, Hydrodynamic and chemical scaling for blow-off dynamics of lean premixed flames stabilized on a meso-scale bluff-body, *Proc. Combust. Inst.* 37 (2019) 1831–1841.
- [9] X. Kang, R. J. Gollan, P. A. Jacobs, A. Veeraragavan, Suppression of instabilities in a premixed methane–air flame in a narrow channel via hydrogen/carbon monoxide addition, *Combust. Flame* 173 (2016) 266–275.
- [10] R. Schefer, D. Wicksall, A. Agrawal, Combustion of hydrogen-enriched methane in a lean premixed swirl-stabilized burner, *Proc. Combust. Inst.* 29 (2002) 843–851.
- [11] F. Cozzi, A. Coghe, Behavior of hydrogen-enriched non-premixed swirled natural gas flames, *Int. J. Hydrogen Energy* 31 (2006) 669–677.
- [12] H. S. Kim, V. K. Arghode, M. B. Linck, A. K. Gupta, Hydrogen addition effects in a confined swirl-stabilized methane-air flame, *Int. J. Hydrogen Energy* 34 (2009) 1054–1062.
- [13] T. Guiberti, D. Durox, P. Scoufflaire, T. Schuller, Impact of heat loss and hydrogen enrichment on the shape of confined swirling flames, *Proc. Combust. Inst.* 35 (2015) 1385–1392.
- [14] S. Shanbhogue, Y. Sanusi, S. Taamallah, M. Habib, E. Mokheimer, A. Ghoniem, Flame macrostructures, combustion instability and extinction strain scaling in swirl-stabilized premixed CH₄/H₂ combustion, *Combust. Flame* 163 (2016) 494–507.
- [15] P. Benard, V. Moureau, G. Lartigue, Y. D’Angelo, Large-Eddy Simulation of a hydrogen enriched methane/air meso-scale combustor, *Int. J. Hydrogen Energy* 42 (2017) 2397–2410.
- [16] D. Cicoria, C. Chan, Large eddy simulation of lean turbulent hydrogen-enriched methane-air premixed flames at high Karlovitz numbers, *Int. J. Hydrogen Energy* 41 (2016) 22479–22496.
- [17] R. Mercier, T. Guiberti, A. Chatelier, D. Durox, O. Gicquel, N. Darabiha, T. Schuller, B. Fiorina, Experimental and numerical investigation of the influence of thermal boundary conditions on premixed swirling flame stabilization, *Combust. Flame* 171 (2016) 42–58.
- [18] D. Moëll, D. Lörstard, X.-S. Bai, LES of Hydrogen Enriched Methane/Air Combustion in the SGT-800 Burner at Real Engine Conditions, in: *Asme Turbo Expo 2018, GT2018-76434*.
- [19] R. Hilbert, F. Tap, H. El-Rabii, D. Thévenin, Impact of detailed chemistry and transport models on turbulent combustion simulations, *Prog. Energy Combust. Sci.* 30 (2004) 61–117.
- [20] G. Oztarlik, L. Selle, T. Poinso, T. Schuller, Suppression of instabilities of swirled premixed flames with minimal secondary hydrogen injection, *Combust. Flame* 214 (2020) 266–276.
- [21] T. Jaravel, E. Riber, B. Cuenot, G. Bulat, Large Eddy Simulation of an industrial gas turbine combustor using reduced chemistry with accurate pollutant prediction, *Proc. Combust. Inst.* 36 (2017) 3817–3825.
- [22] F. Nicoud, H. B. Toda, O. Cabrit, S. Bose, J. Lee, Using singular values to build a subgrid-scale model for large eddy simulations, *Phys. Fluids* 23 (2011) 85106.
- [23] O. Colin, M. Rudgyard, Development of high-order Taylor-galerkin schemes for LES, *J. Comput. Phys.* 162 (2000) 338–371.
- [24] T. J. Poinso, S. Lelef, Boundary conditions for direct simulations of compressible viscous flows, *J. Comput. Phys.* 101 (1992) 104–129.
- [25] J. F. Grcar, J. B. Bell, M. S. Day, The Soret effect in naturally propagating, premixed, lean, hydrogen–air flames, *Proc. Combust. Inst.* 32 (2009) 1173–1180.
- [26] T. Poinso, D. Veynante, *Theoretical and numerical combustion*, RT Edwards, Inc., 2005.
- [27] H. Yamashita, M. Shimada, T. Takeno, A numerical study on flame stability at the transition point of jet diffusion flames, *Symp. Combust.* 26 (1996) 27–34.
- [28] A. L. Sánchez, F. A. Williams, Recent advances in understanding of flammability characteristics of hydrogen, *Prog. Energy Combust. Sci.* 41 (2014) 1–55.